Dynamical Spectra of Spin Supersolid States in Triangular Antiferromagnets

Runze Chi,[1,2] Jiahang Hu,[1,2] Hai-Jun Liao,[1,3,*] and T. Xiang[1,2,4,†]

[1] *Beijing National Laboratory for Condensed Matter Physics and Institute of Physics, Chinese Academy of Sciences, Beijing 100190, China.*
[2] *School of Physical Sciences, University of Chinese Academy of Sciences, Beijing 100049, China.*
[3] *Songshan Lake Materials Laboratory, Dongguan, Guangdong 523808, China.*
[4] *Beijing Academy of Quantum Information Sciences, Beijing, 100190, China.*

We employ tensor network renormalization to explore the dynamical spectra of the easy-axis triangular-lattice antiferromagnet (TLAF) in a magnetic field. Our analysis identifies two distinct low-energy magnon excitations: a gapless Goldstone mode and a gapped mode. At zero field, the spectra display two nearly degenerate roton modes near the M point. With the increase of the magnetic field within the Y-shape superfluid phase, these modes diverge, with the roton excitation vanishing from the Goldstone mode branch, suggesting that the roton dip in this mode may just result from the energy-level repulsion imposed by the roton excitation in the gapped mode. Moreover, the in-plane spectral function shows substantial weight in high energies in the same spin excitation channel where the low-energy roton excitation appears. However, these roton excitations are absent in the V-shape supersolid phase.

arXiv:2404.14163v1 [cond-mat.str-el] 22 Apr 2024

Introduction— The quest to understand supersolidity, a remarkable state featuring both spatial order and superfluidity, has captivated researchers across disciplines. Originating from the study of solid helium-4 [1], this enigmatic phenomenon has extended its reach to diverse systems, including ultracold gases [2–7] and hard-core bosons [8–12]. A promising avenue for exploring supersolidity lies in the easy-axis S=1/2 triangular-lattice antiferromagnet (TLAF) [13–15], where the spin states of magnetic ions mirror the occupancy states of lattice sites by Bose atoms. The ground state of the easy-axis TLAF, characterized by the spontaneous breaking of lattice translation and spin rotational symmetries, bears a resemblance to the supersolid state of Bose atoms.

Recently, this elusive supersolid phase has been observed in the easy-axis triangular-lattice antiferromagnet $Na_2BaCo(PO_4)_2$, exhibiting a notable magnetocaloric effect [16]. Early thermodynamic measurements down to 50 mK at zero magnetic field [17, 18] suggested that $Na_2BaCo(PO_4)_2$ might be a candidate material for a quantum spin liquid (QSL). However, subsequent research [19, 20] revealed that at around 150 mK, $Na_2BaCo(PO_4)_2$ undergoes a transition from paramagnetic to antiferromagnetic state. Moreover, due to the small exchange interactions in $Na_2BaCo(PO_4)_2$, a moderate magnetic field can drive it into a fully polarized state. As a result, comprehensive inelastic neutron scattering measurements [20, 21] have been conducted to explore its complete phase diagram under applied magnetic fields, including the Y-shape, up-up-down (UUD), V-shape, and fully polarized phases, where the Y-shape and V-shape phases possess supersolid order. The synthesis of other candidate materials for supersolid phases, such as $K_2Co(SeO_3)_2$ [22, 23], has also invigorated research in this field.

Despite these advancements, there remains a gap in understanding excitations of supersolid states in the easy-axis TLAF. While $Na_2BaCo(PO_4)_2$ exhibits clear long-range magnetic order at low-temperature [19, 20], the recent neutron scattering experiments [21] have revealed that, unlike the semiclassical spin wave theory predictions, its low-energy excitation spectrum lacks sharp magnon excitations and instead exhibits a broad continuum resembling deconfined fractional spinon excitations, suggesting the possibility of proximate quantum spin-liquid states [24]. Consequently, there is an urgent need for further theoretical exploration to determine the intrinsic nature of these spectral features and illuminate the elusive phenomenon of supersolidity.

To address these challenges, we conduct a comprehensive numerical investigation into the dynamical excitations of the easy-axis TLAF in a magnetic field by the tensor network method. We find that two sharp magnon excitation modes emerge at low energy: a gapless Goldstone mode and a gapped mode. Furthermore, two nearly degenerate roton or roton-like magnon excitation modes at M point are observed. As the magnetic field increases, the two nearly degenerate roton modes gradually separate, and the the roton mode from the lowest branch with Goldstone mode transitions from a dip to a hump shape, suggesting that the roton dip in this mode may just result from the energy-level repulsion imposed by the roton excitation in the second lowest branch. While another roton excitation persists throughout the entire Y-shape phase. Furthermore, the in-plane spectral function shows substantial high-energy spectral weight in the same spin excitation channel where this roton excitation appears, suggesting that the second branch of roton excitation stems from the magnon-Higgs scattering mechanism [25]. Finally, these roton excitations are absent in the V-shape supersolid phase.

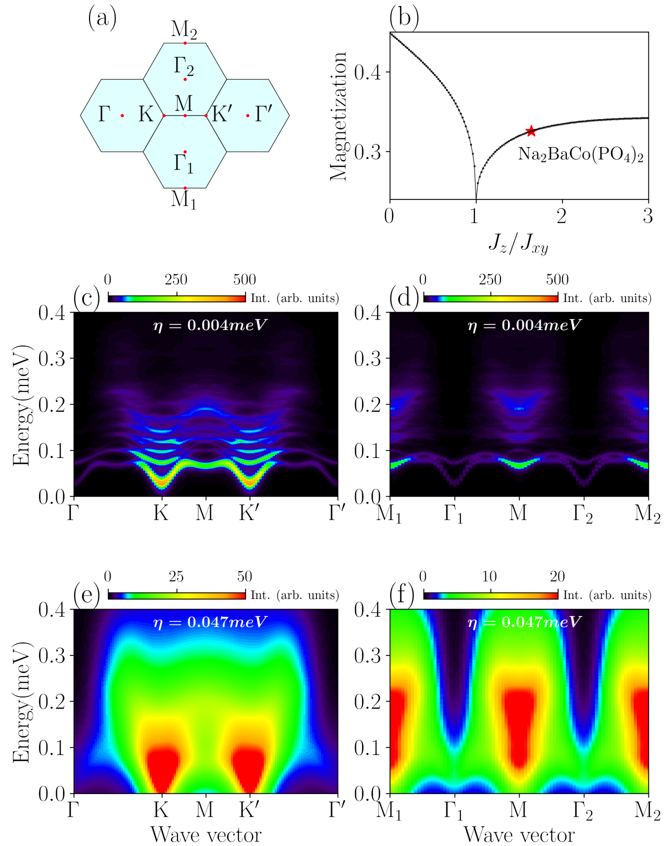

FIG. 1. Zero-field spectral functions with two different Lorentzian broadening factors η along two momentum paths. (a) Schematic diagram of the Brillouin zone. (b) Magnetization of LSWT as a function of anisotropic ratio J_z/J_{xy}, where the red star is corresponding to $Na_2BaCo(PO_4)_2$. (c-d) The spectral functions with $\eta = 0.004$ meV (about 0.053 J_{xy}) along Γ-K-M-K′-Γ' and M_1-Γ_1-M-Γ_2-M_2, respectively. (e-f) The spectral functions along two directions with $\eta = 0.047$ meV (about 0.62 J_{xy}), which is equal to the experimental energy resolution [21].

Model and method— We here consider the easy-axis triangular-lattice antiferromagnetic XXZ model

$$\mathcal{H}=\sum_{\langle ij\rangle}[J_z S_i^z S_j^z + J_{xy}\left(S_i^x S_j^x + S_i^y S_j^y\right)] - g_z\mu_B B\sum_i S_i^z, \quad (1)$$

where $\langle ij\rangle$ runs over all the nearest-neighbor sites of the two-dimensional triangular lattice, and $J_z > J_{xy}$. The ground-state phase diagram of this model has been studied [14, 26]. As the magnetic field increases, as shown in Fig. 2(a), the ground state of this model undergoes transitions through the Y-shape phase, up-up-down (UUD) phase, V-shape phase, and fully polarized phase. Among them, the Y- and V-shape phases are spin supersolid phases [15, 16]. In this work, we adopt typical anisotropic parameters $J_{xy} = 0.076$ meV, $J_z = 0.125$ meV and $g_z = 4.645$, which are believed to precisely describe the supersolid material of the easy-axis triangular antiferromagnet $Na_2BaCo(PO_4)_2$ [21]. Although the following discussion focuses on a specific material, the outcomes are applicable to other easy-axis triangular antiferromagnets that have the same phase diagram.

To simulate the spin excitation spectra of neutron scattering experiment, we utilize the state-of-art tensor-network method [27–31], based on the single-mode excited tensor network representation [32] and automatic differentiation [33], to calculate the spin spectral function

$$S^{tot}(\boldsymbol{k},\omega) = \sum_\alpha S^{\alpha\alpha}(\boldsymbol{k},\omega), \quad (\alpha = x, y, z),$$
$$S^{\alpha\beta}(\boldsymbol{k},\omega) = \langle 0|S^\alpha_{-\boldsymbol{k}}\delta(\omega - H + E_0)S^\beta_{\boldsymbol{k}}|0\rangle. \quad (2)$$

This method has recently been successfully applied to the easy-plane triangular-lattice antiferromagnet $Ba_3CoSb_2O_9$ [31], and quantitatively accounts for its neutron scattering experimental results. Further details on this method can be found in the Supplemental Material (SM) and Refs. [30, 31].

In the calculation, the delta function is expanded by a Lorentzian broadening factor η, which can mimic the broadening effect by the instrument energy resolution in neutron scattering experiment. It is crucial to distinguish whether the low-energy continuum spectrum is intrinsic or caused by finite instrumental resolution.

Results— Figure 1 shows the zero-field spin excitation spectra with different Lorentzian broadening factor η along Γ-K-M-K′-Γ' and M_1-Γ_1-M-Γ_2-M_2. As shown in Fig. 1(c) and (d), sharp magnon excitations are observed along both directions in the low-energy excitation spectra, consistent with the conventional expectations for the low-energy excitations of magnetically ordered systems but inconsistent with the low-energy continuum spectra observed in recent neutron scattering experiments [21]. To account for this discrepancy, we investigated the excitation spectra using a broadening factor of 0.047 meV (about 0.62 J_{xy}), corresponding to the energy resolution of recent neutron scattering experiment [21]. Under this condition, as shown in Fig. 1(e) and (f), the spin excitation spectra exhibit obvious low-energy continuum, similar to the experimental results. Besides, we analyzed the variation of magnetization with anisotropy and found that regardless of whether it's easy-plane or easy-axis anisotropy, the magnetization is always enhanced as it deviates from the isotropic Heisenberg point (see Fig. 1(b)). This indicates that magnetic anisotropies tend to stabilize magnetic order rather than suppress it, suggesting that $Na_2BaCo(PO_4)_2$ is further away from the U(1) Dirac spin liquid phase compared to the Heisenberg point. Therefore, these results suggest that the low-energy continuum spectra observed in the experiment are not intrinsic but likely caused by broadening effects due to instrumental resolution or other factors.

Furthermore, we find that these two low-energy magnon excitations can be distinguished by different

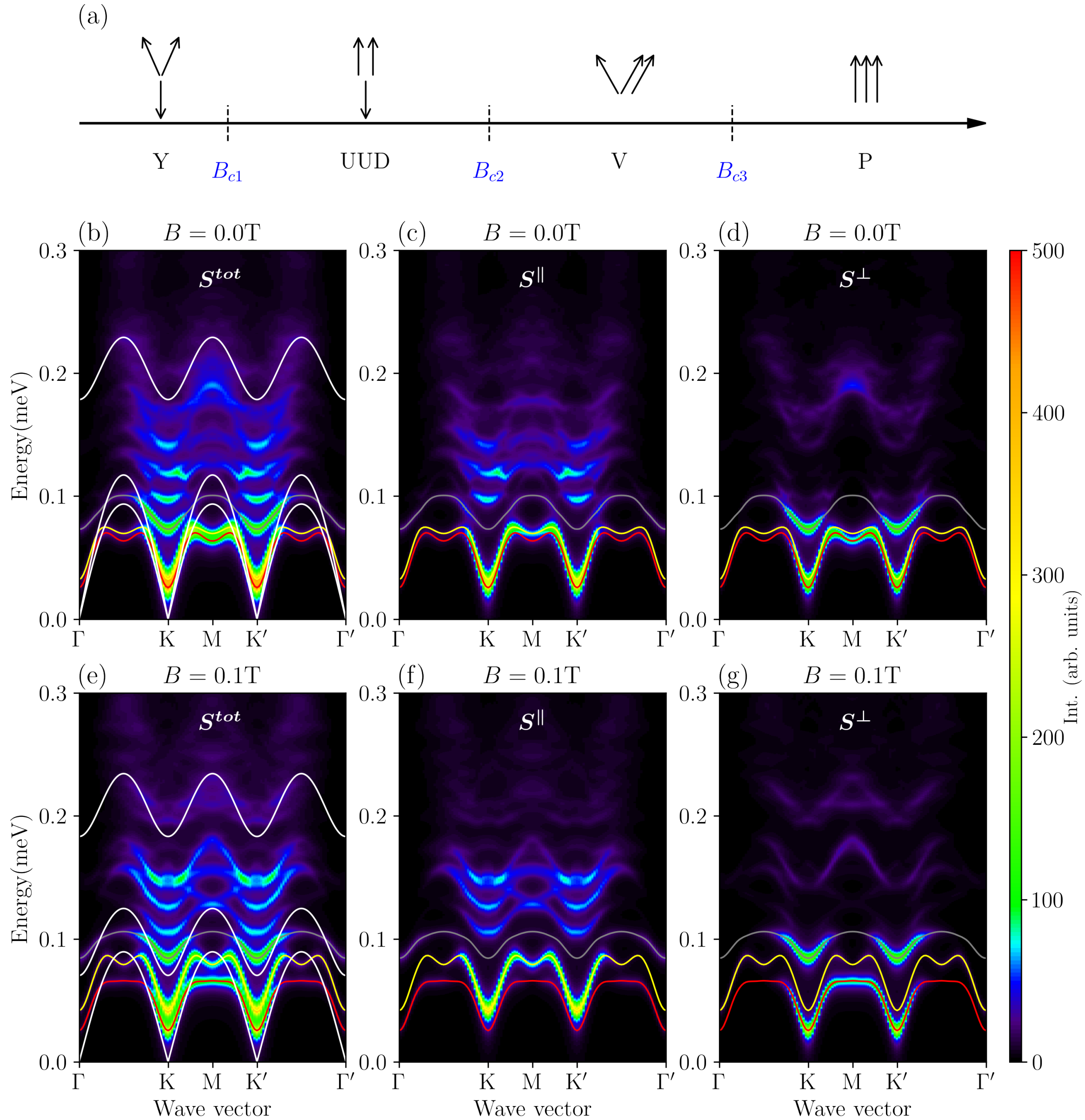

FIG. 2. The dynamical spectral functions with $\eta = 0.004$ meV in the Y-shape supersolid phase. (a) The phase diagram of the easy-axis TLAF. For $Na_2BaCo(PO_4)_2$ with $J_{xy} = 0.076$ meV, $J_z = 0.125$ meV and $g_z = 4.645$, the three critical points are $B_{c1} = 0.42$ T, $B_{c2} = 1.13$ T, and $B_{c3} = 1.8$ T, respectively. (b)-(d) The spectral function at zero field. (e)-(g) The spectal function with $B = 0.1$ T. (b) and (e) show the total spectral functions $S^{tot}(\boldsymbol{k}, \omega)$, where the white lines denote the LSWT results, and the red, yellow, and gray lines correspond to the lowest-energy three branches of magnon excitations obtained by tensor network method, respectively. (c) and (f) show the in-plane spectral function $S^{\parallel}(\boldsymbol{k}, \omega) = S^{xx}(\boldsymbol{k}, \omega) + S^{zz}(\boldsymbol{k}, \omega)$. (d) and (g) are the out-of-plane spectral function $S^{\perp}(\boldsymbol{k}, \omega) = S^{yy}(\boldsymbol{k}, \omega)$, which probes the Goldstone mode.

components of spectral function. As shown in Fig. 2 (d) and (g), the lowest-energy magnon excitation (red curve) predominantly appears in the out-of-plane spectral function

$$S^{\perp}(\boldsymbol{k}, \omega) = S^{yy}(\boldsymbol{k}, \omega), \tag{3}$$

while the next lowest-energy magnon excitation (yellow curve) mainly appears in the in-plane spectral function (see Fig. 2 (c) and (f))

$$S^{\parallel}(\boldsymbol{k}, \omega) = S^{xx}(\boldsymbol{k}, \omega) + S^{zz}(\boldsymbol{k}, \omega). \tag{4}$$

The out-of-plane spectral function represents transverse fluctuations perpendicular to the xz-plane of magnetic order. Therefore, it should exhibit a gapless Goldstone mode at the K point. The reason why the lowest-energy branch (red curve) shows a finite gap at the K point is that the tensor network method introduces a trun-

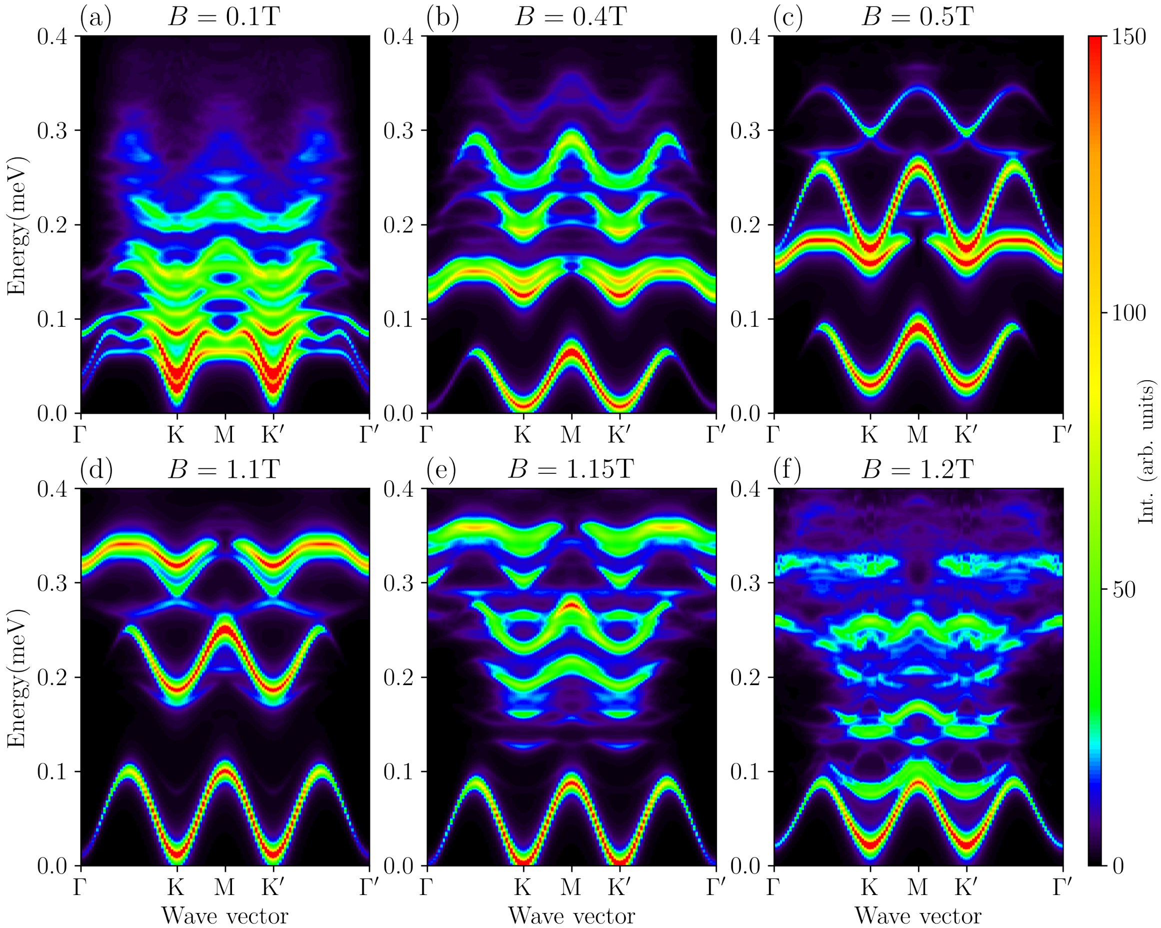

FIG. 3. Comparison of the spectral functions with $\eta = 0.004$ meV between the two supersolid phases and UUD phase. (a)-(b) The spectral functions in the Y-shape supersolid phase at magnetic fields $B = 0.1$ T and $B = 0.4$ T, respectively. (c)-(d) The spectral functions in the UUD phase with magnetic fields $B = 0.5$ T and $B = 1.1$ T, respectively. (e)-(f) The spectral functions in the V-shape supersolid phase with magnetic fields $B = 1.15$ T and $B = 1.2$ T, respectively.

cation parameter D, which leads to a finite correlation length of the ground state, resulting in a finite excitation gap. Practical computations [28–31, 34, 35] have demonstrated that this gap induced by finite D systematically decreases and gradually vanishes with increasing D (see Fig. S2 in the Sec. II of SM), thereby satisfying the Goldstone theorem. As shown by the white curves in Fig. 2(b), LSWT predicts that there are two gapless magnon excitations around K point [36], where the first branch is the well-known Goldstone mode due to breaking the U(1) symmetry of the Hamiltonian Eq. (1), and the second gapless mode is because the classical ground state possesses an additional U(1) rotational symmetry around the y-axis (where the spins are aligned in the xz-plane) [36]. The second gapless mode only exists within the linear spin-wave approximation. In the presence of quantum fluctuation or magnetic field, as shown in Fig. 2(c) and (f), the ground state no longer exhibits additional U(1) rotational symmetry around the y-axis, and thus the second-lowest branch acquires a finite gap, which is about 0.01 meV at zero field (see Fig. S2 of SM).

More importantly, the low-energy excitation spectrum at zero field exhibits two nearly degenerate branches of roton excitation modes (an elementary excitation first seen in superfluid helium-4) with a minimum at M point. It can be seen from Fig. 2(c-d) that these two nearly degenerate roton excitation modes are one-to-one connected to the lowest-energy Goldstone mode and the second lowest-energy gapped mode at K point. Besides superfluid helium-4, the roton excitation has also been observed in the triangular antiferromagnet $Ba_3CoSb_2O_9$ [37, 38] and square-lattice antiferromagnet [39]. There have been many theoretical attempts to explain the origin of roton excitation, such as the fractional spinon theory [40–43], vortex–antivortex pair [44, 45], avoid quasiparticle decay [46] and magnon-Higgs scattering [25, 31, 47]. As shown in Fig. 2 (d), the roton excitation in the branch of Goldstone mode (red curve) stems from the out-of-plane fluctuation $S^{\perp}(\boldsymbol{k}, \omega)$. It quickly separates from the second lowest branch and disappears with the increasing of magnetic field (see Fig. S4 (k-o)), suggesting that it arises from the energy-level repulsion induced by the roton excitation in the second lowest branch. While another roton excitation in the second lowest branch (yellow curve) arises from the in-plane fluctuation $S^{\parallel}(\boldsymbol{k},\omega)$ (see Fig. 2 (c)), and it still persists in the whole Y phase (see Fig. S4 (f-j)). Besides, the in-plane spectral function shows substantial high-energy spectral weight in the same spin excitation channel where this roton excitation appears, suggesting that the emergence of the this roton excitation is more likely attributable to the strong magnon-Higgs scattering mechanism [25] between the in-plane transverse magnon mode and the in-plane longitudinal Higgs mode.

To further demonstrate the existence of strong magnetic-Higgs scattering in the supersolid phase, we compare the excitation spectra between two supersolid phases and the UUD phase near their phase boundaries. In the UUD phase, since all spins of the ground state are aligned collinearly, there are no three-magnon interaction terms in the spin wave expansion, resulting in weak coupling between transverse and longitudinal fluctuation modes and, thus, no prominent continuum spectra (see Fig. 3 (c) and (d)). However, once entering the supersolid phases, the high-energy excitation spectra in the two supersolid phases begin to become more diffusive. The further away from the UUD phase, the more severe the diffusion becomes (see Fig. 3 (a-b) and (e-f)). This is because the spins of the ground state are non-collinearly arranged in both the Y-shape and V-shape supersolid phases, the three-magnon interaction term inevitably appears in the spin-wave expansion. This leads to strong coupling between transverse magnon mode and longitudinal Higgs mode, thereby resulting in continuum spectra. In addition, we also note that the low-energy excitation spectra in the V-shape supersolid phase do not exhibit roton excitations, indicating that roton excitations are not a necessary condition for the onset of supersolid order, unlike in traditional superfluid helium-4.

Discussion— This work presents a comprehensive numerical investigation into the dynamical excitations of the easy-axis triangular-lattice antiferromagnets under a magnetic field, employing the tensor network method. The study reveals that sharp magnon excitations emerge at low energies, indicating that the observed low-energy continuum spectra likely stem from broadening effects of the instrumental energy resolution, especially when exchange interaction is weak. It reminds us to be very cautious when a magnetic material with relatively weak exchange interactions exhibits low-energy continuum spectra in neutron scattering experiments. The low-energy continuum may not necessarily be a signature of fractionalized spinon excitations, but could also be due to broadening effects caused by other factors.

Moreover, we find two branches of roton excitations at zero field. The roton excitation in the branch of Goldstone mode is rapidly destroyed by the magnetic field. Conversely, the roton excitation arising from in-plane fluctuations remains stable throughout the entire Y-shape phase under the influence of the magnetic field. Further insights from the in-plane spectral function reveal a close connection between the roton excitations and high-energy continuum spectra, suggesting that the roton excitations are caused by the mechanism of strong magnon-Higgs scattering [25]. On the other hand, the absence of roton-like excitations in the V-shape supersolid phase suggests that it is not inherently linked to the spin supersolid phase. These findings not only enhance our understanding of spin dynamics in TLAFs but also provide new insights into the underlying mechanism of supersolid states, paving the way for potential applications that leverage the novel properties of supersolid states.

Acknowledgements We thank Yuan Wan and Wei Li for the helpful discussion. This work is supported by the Strategic Priority Research Program of Chinese Academy of Sciences (Grants No. XDB0500202, XDB33010100 and No. XDB33020300), the National Natural Science Foundation of China (Grants No. 12322403, No. 12347107, No. 12488201, No. 11874095, and No. 11974396), the National Key Research and Development Project of China (Grants No. 2022YFA1403900 and No. 2017YFA0302901) and the Youth Innovation Promotion Association of Chinese Academy of Sciences (Grant No. 2021004).

* navyphysics@iphy.ac.cn
† txiang@iphy.ac.cn

[1] A. J. Leggett, Phys. Rev. Lett. **25**, 1543 (1970).
[2] M. Boninsegni and N. V. Prokof'ev, Rev. Mod. Phys. **84**, 759 (2012).
[3] Z.-K. Lu, Y. Li, D. S. Petrov, and G. V. Shlyapnikov, Phys. Rev. Lett. **115**, 075303 (2015).
[4] J.-R. Li, J. Lee, W. Huang, S. Burchesky, B. Shteynas, F. Ç. Top, A. O. Jamison, and W. Ketterle, Nature **543**, 91 (2017).
[5] J. Léonard, A. Morales, P. Zupancic, T. Donner, and T. Esslinger, Science **358**, 1415 (2017).
[6] L. Tanzi, S. M. Roccuzzo, E. Lucioni, F. Famà, A. Fioretti, C. Gabbanini, G. Modugno, A. Recati, and S. Stringari, Nature **574**, 382 (2019).
[7] M. A. Norcia, C. Politi, L. Klaus, E. Poli, M. Sohmen, M. J. Mark, R. N. Bisset, L. Santos, and F. Ferlaino, Nature **596**, 357 (2021).
[8] S. Wessel and M. Troyer, Phys. Rev. Lett. **95**, 127205 (2005).
[9] R. G. Melko, A. Paramekanti, A. A. Burkov, A. Vishwanath, D. N. Sheng, and L. Balents, Phys. Rev. Lett. **95**, 127207 (2005).

[10] D. Heidarian and K. Damle, Phys. Rev. Lett. **95**, 127206 (2005).

[11] M. Boninsegni and N. Prokof'ev, Phys. Rev. Lett. **95**, 237204 (2005).

[12] F. Wang, F. Pollmann, and A. Vishwanath, Phys. Rev. Lett. **102**, 017203 (2009).

[13] D. Heidarian and A. Paramekanti, Phys. Rev. Lett. **104**, 015301 (2010).

[14] D. Sellmann, X.-F. Zhang, and S. Eggert, Phys. Rev. B **91**, 081104 (2015).

[15] Y. Gao, Y.-C. Fan, H. Li, F. Yang, X.-T. Zeng, X.-L. Sheng, R. Zhong, Y. Qi, Y. Wan, and W. Li, npj Quantum Mater. **7**, 89 (2022).

[16] J. Xiang, C. Zhang, Y. Gao, W. Schmidt, K. Schmalzl, C.-W. Wang, B. Li, N. Xi, X.-Y. Liu, H. Jin, G. Li, J. Shen, Z. Chen, Y. Qi, Y. Wan, W. Jin, W. Li, P. Sun, and G. Su, Nature **625**, 270 (2024).

[17] R. Zhong, S. Guo, G. Xu, Z. Xu, and R. J. Cava, Proc. Natl. Acad. Sci. U. S. A. **116**, 14505 (2019).

[18] S. Lee, C. H. Lee, A. Berlie, A. D. Hillier, D. T. Adroja, R. Zhong, R. J. Cava, Z. H. Jang, and K.-Y. Choi, Phys. Rev. B **103**, 024413 (2021).

[19] N. Li, Q. Huang, X. Y. Yue, W. J. Chu, Q. Chen, E. S. Choi, X. Zhao, H. D. Zhou, and X. F. Sun, Nat. Commun. **11**, 4216 (2020).

[20] J. Sheng, L. Wang, A. Candini, W. Jiang, L. Huang, B. Xi, J. Zhao, H. Ge, N. Zhao, Y. Fu, J. Ren, J. Yang, P. Miao, X. Tong, D. Yu, S. Wang, Q. Liu, M. Kofu, R. Mole, G. Biasiol, D. Yu, I. A. Zaliznyak, J.-W. Mei, and L. Wu, Proc. Natl. Acad. Sci. U. S. A. **119**, e2211193119 (2022).

[21] J. Sheng, L. Wang, W. Jiang, H. Ge, N. Zhao, T. Li, M. Kofu, D. Yu, W. Zhu, J.-W. Mei, Z. Wang, and L. Wu, (2024), arXiv:2402.07730 [cond-mat.str-el].

[22] M. Zhu, V. Romerio, N. Steiger, N. Murai, S. Ohira-Kawamura, K. Y. Povarov, Y. Skourski, R. Sibille, L. Keller, Z. Yan, S. Gvasaliya, and A. Zheludev, (2024), arXiv:2401.16581 [cond-mat.str-el].

[23] T. Chen, A. Ghasemi, J. Zhang, L. Shi, Z. Tagay, L. Chen, E.-S. Choi, M. Jaime, M. Lee, Y. Hao, H. Cao, B. Winn, R. Zhong, X. Xu, N. P. Armitage, R. Cava, and C. Broholm, (2024), arXiv:2402.15869 [cond-mat.str-el].

[24] H. Jia, B. Ma, Z. Wang, and G. Chen, Quantum spin supersolid as a precursory dirac spin liquid in a triangular lattice antiferromagnet (2023), arXiv:2304.11716 [cond-mat.str-el].

[25] M. Powalski, G. S. Uhrig, and K. P. Schmidt, Phys. Rev. Lett. **115**, 207202 (2015).

[26] D. Yamamoto, G. Marmorini, and I. Danshita, Phys. Rev. Lett. **112**, 127203 (2014).

[27] L. Vanderstraeten, M. Mariën, F. Verstraete, and J. Haegeman, Phys. Rev. B **92**, 201111 (2015).

[28] L. Vanderstraeten, J. Haegeman, and F. Verstraete, Phys. Rev. B **99**, 165121 (2019).

[29] B. Ponsioen and P. Corboz, Phys. Rev. B **101**, 195109 (2020).

[30] B. Ponsioen, F. F. Assaad, and P. Corboz, SciPost Phys. **12**, 006 (2022).

[31] R. Chi, Y. Liu, Y. Wan, H.-J. Liao, and T. Xiang, Phys. Rev. Lett. **129**, 227201 (2022).

[32] S. Östlund and S. Rommer, Phys. Rev. Lett. **75**, 3537 (1995).

[33] H.-J. Liao, J.-G. Liu, L. Wang, and T. Xiang, Phys. Rev. X **9**, 031041 (2019).

[34] W.-L. Tu, L. Vanderstraeten, N. Schuch, H.-Y. Lee, N. Kawashima, and J.-Y. Chen, PRX Quantum **5**, 010335 (2024).

[35] K. Wang, S. Feng, P. Zhu, R. Chi, H.-J. Liao, N. Trivedi, and T. Xiang, (2024), arXiv:2403.12141 [cond-mat.str-el].

[36] B. Kleine, E. Müller-Hartmann, K. Frahm, and P. Fazekas, Z. Physik B - Condensed Matter **87**, 103 (1992).

[37] S. Ito, N. Kurita, H. Tanaka, S. Ohira-Kawamura, K. Nakajima, S. Itoh, K. Kuwahara, and K. Kakurai, Nat. Commun. **8**, 235 (2017).

[38] D. Macdougal, S. Williams, D. Prabhakaran, R. I. Bewley, D. J. Voneshen, and R. Coldea, Phys. Rev. B **102**, 064421 (2020).

[39] B. Dalla Piazza, M. Mourigal, N. B. Christensen, G. J. Nilsen, P. Tregenna-Piggott, T. G. Perring, M. Enderle, D. F. McMorrow, D. A. Ivanov, and H. M. Rønnow, Nat. Phys. **11**, 62 (2015).

[40] W. Zheng, J. O. Fjærestad, R. R. P. Singh, R. H. McKenzie, and R. Coldea, Phys. Rev. Lett. **96**, 057201 (2006).

[41] C. Zhang and T. Li, Phys. Rev. B **102**, 075108 (2020).

[42] F. Ferrari and F. Becca, Phys. Rev. X **9**, 031026 (2019).

[43] E. A. Ghioldi, S.-S. Zhang, Y. Kamiya, L. O. Manuel, A. E. Trumper, and C. D. Batista, Phys. Rev. B **106**, 064418 (2022).

[44] H. Li, Y. D. Liao, B.-B. Chen, X.-T. Zeng, X.-L. Sheng, Y. Qi, Z. Y. Meng, and W. Li, Nat. Commun. **11**, 1111 (2020).

[45] J. Alicea, O. I. Motrunich, and M. P. A. Fisher, Phys. Rev. B **73**, 174430 (2006).

[46] R. Verresen, R. Moessner, and F. Pollmann, Nat. Phys. **15**, 750 (2019).

[47] A. L. Chernyshev and M. E. Zhitomirsky, Phys. Rev. B **79**, 144416 (2009).

Supplementary material

Dynamical Spectra of Spin Supersolid States in Triangular Antiferromagnets

Runze Chi,[1,2] Jiahang Hu,[1,2] Hai-Jun Liao,[1,3,*] and T. Xiang[1,2,4,†]

[1]*Beijing National Laboratory for Condensed Matter Physics and Institute of Physics, Chinese Academy of Sciences, Beijing 100190, China.*
[2]*School of Physical Sciences, University of Chinese Academy of Sciences, Beijing 100049, China.*
[3]*Songshan Lake Materials Laboratory, Dongguan, Guangdong 523808, China.*
[4]*Beijing Academy of Quantum Information Sciences, Beijing, China.*

I. TENSOR NETWORK METHOD

In this study, we employ the same infinite projected entangled-pair state (iPEPS) as Ref. [R1] to represent the ground state

$|0\rangle =$ 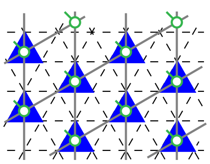 $=$ 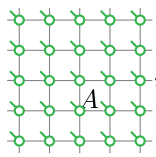 , (Q1)

where we group three sites on a triangle into one site, making the original triangular lattice to a deformed square lattice. Each local tensor A is composed of one physical index of dimension $d = 8$ and four virtual indices of dimension D, which controls the accuracy of the calculation. The local tensor A can be determined by variational minimization of the ground state energy via automatic differentiation techniques [R2]. This wave function representation is compatible with all ground states of the easy-axis triangular-lattice antiferromagnetic XXZ model with a magnetic field, including the Y-shape, V-shape, up-up-down and fully polarized states.

To calculate spectral function, we construct a set of excited states $|\Phi_{\boldsymbol{k}}(B_m)\rangle$ with a definite momentum k [R1, R3–R6], which are orthogonal to the ground state by replacing a local tensor A at site $\boldsymbol{r}$ of the ground state $|\Psi(A)\rangle$ with a new tensor B_m shown as follows

$|m\rangle \equiv |\Phi_{\boldsymbol{k}}(B_m)\rangle = \sum_{\boldsymbol{r}} e^{i\boldsymbol{k}\cdot\boldsymbol{r}}$ 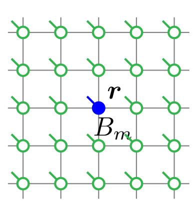 . (Q2)

Then, we compute the effective Hamiltonian $H^{\text{eff}}_{mn} = \langle\Phi_{\boldsymbol{k}}(B_m)|H|\Phi_{\boldsymbol{k}}(B_n)\rangle$ and the overlap matrix $N_{mn} = \langle\Phi_{\boldsymbol{k}}(B_m)|\Phi_{\boldsymbol{k}}(B_n)\rangle$ in this set of excited-state basis, and solve their generalized eigen-equation to obtain the excited energies $\{E_m\}$ and wavefunctions $\{|m\rangle\}$. Finally, we can obtain the zero-temperature dynamical spectral function

$$S^{\alpha\beta}(\boldsymbol{k},\omega) = \sum_m \langle 0|S^{\alpha}_{-\boldsymbol{k}}|m\rangle\langle m|S^{\beta}_{\boldsymbol{k}}|0\rangle\delta(\omega - E_m + E_0). \tag{Q3}$$

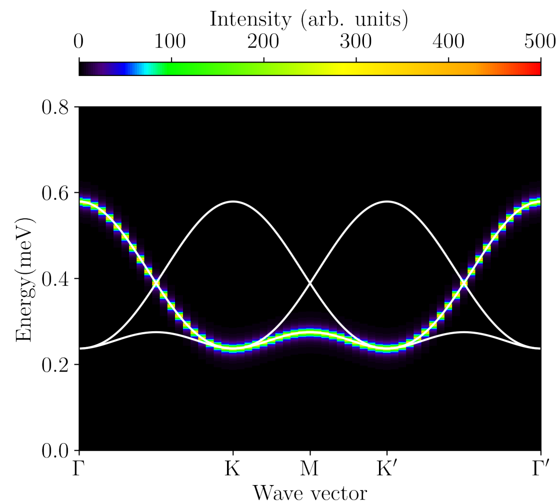

FIG. S1. The spectral function of the fully polarized state at magnetic field $B = 2.7$ T. The white lines denote the LSWT results. The tensor network results (solid squares) are obtained with bond dimension $D = 4$.

This method has been demonstrated to accurately obtain excitation spectra of frustrated magnetic systems [R1, R4–R7]. Here, we also benchmark the excitation spectra of fully polarized phases as shown in Fig. S1, and observe perfect agreement with the results from linear spin wave theory [R8], which is the exact solution for a fully polarized state because the fully polarized state does not involve quantum fluctuations. All our calculations were carried out using bond dimension $D = 4$ and Lorentz broading factor $\eta = 0.004$ meV if not specified otherwise.

II. BOND DIMENSION DEPENDENCE OF THE TWO LOWEST ENERGY GAPS

The antiferromagnetic XXZ model has a continuous U(1) symmetry, and should have a gapless Goldstone mode according to the Goldstone theorem. The reason why the lowest-energy branch in our results has a finite gap at the K point

* navyphysics@iphy.ac.cn
† txiang@iphy.ac.cn

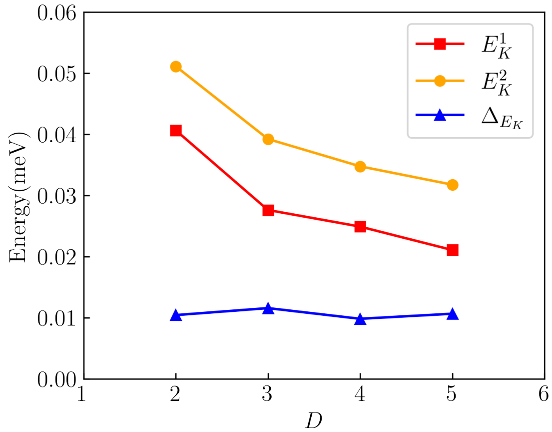

FIG. S2. The lowest and second lowest energy excited gaps at the K point as a function of the bond dimension D of iPEPS.

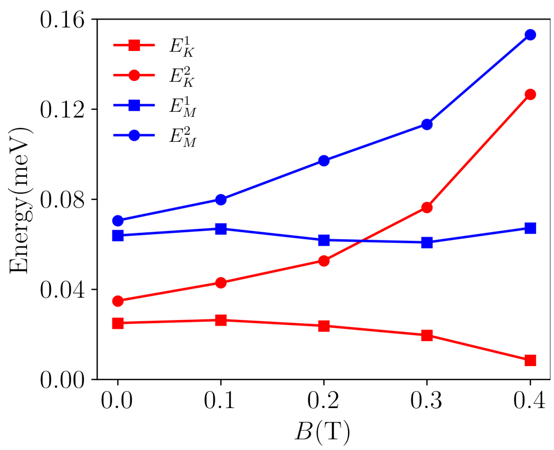

FIG. S3. The lowest (solid squares) and second lowest (solid circles) energy excited gaps at the K (red) and M (blue) points as a function of the magnetic field, respectively.

is because the tensor network method introduces a truncation parameter, the bond dimension D, which leads to a finite correlation length of ground state. Therefore, the excitation is always gapped when the bond dimension D is finite, and becomes gapless only in the limit $D \to \infty$ (namely, $\xi \to \infty$). Practical computations [R1, R4–R7] have demonstrated that this gap induced by finite D systematically decreases and gradually vanishes with increasing of D, thereby satisfying the Goldstone theorem. As shown in Fig. S2, our tensor network results indeed align with the expected outcomes. Both low energy modes at K point gradually decrease with the increasing of bond dimension D. More importantly, they consistently maintain a nearly constant energy spacing of about 0.01 meV (see the blue curve in Fig. S2), indicating that the second branch E_{K}^2 should have an intrinsic finite gap of about 0.01 meV in the limit $D \to \infty$.

III. EVOLUTION OF EXCITATION SPECTRA IN THE Y-SHAPE PHASE WITH MAGNETIC FIELD

Figure S4 illustrates the behaviors of the excitation spectra in the Y-shape supersolid phase as a function of magnetic field, where, as shown in Fig. 2(a) of the main text, the system remains in the Y-shape supersolid state for magnetic fields ranging from 0 T to 0.42 T. To distinguish the contributions of different spin fluctuation channels, we also plot the spectral functions S^{xx}, S^{yy}, and S^{zz}. Since the magnetic order lies in the xz plane, S^{yy} mainly exhibits the out-of-plane transverse fluctuations, while S^{zz} and S^{xx} mainly represent the in-plane fluctuations. As shown in Fig. S4 (k-o), the lowest and third lowest energy branches are primarily influenced by the out-of-plane fluctuations, whereas the second-lowest energy branch arises from the in-plane fluctuations, including the contributions from both the S^{xx} and S^{zz}.

Furthermore, our tensor network results exhibit significant downward renormalization of magnons compared to the results of linear spin wave theory (the white lines in Fig. S4 (a-e)). In particular, the emergence of roton minima at the M point suggests the significant contributions of strong quantum fluctuations. At zero field, the spectra display two nearly degenerate roton excitation modes around the M point. As the magnetic field increases, these modes are away from each other (see Fig. S3), with the roton excitation vanishing from the Goldstone mode branch, suggesting that the roton dip in this mode may just result from the energy-level repulsion imposed by the roton excitations in the second lowest branch. On the other hand, the second lowest energy magnon excitations gradually shift to higher energies with increasing magnetic field, but consistently maintain a roton minimum at the M point. Moreover, the in-plane spectral functions (S^{xx} and S^{zz}) show substantial high-energy spectral weights in the same spin excitation channel where the low-energy roton excitations appear. This indicates the existence of strong hybridization between in-plane transverse and longitudinal fluctuations, suggesting that the second roton excitation may arise from the hybridization of in-plane transverse and longitudinal modes. This can be seen from Fig. S4 (f-j) and (p-t). As the magnetic field increases, the spin alignment gradually orients towards the z direction, leading to a gradual weakening of the coupling between the in-plane transverse and longitudinal modes. Consequently, the depth of the roton minimum also gradually decreases.

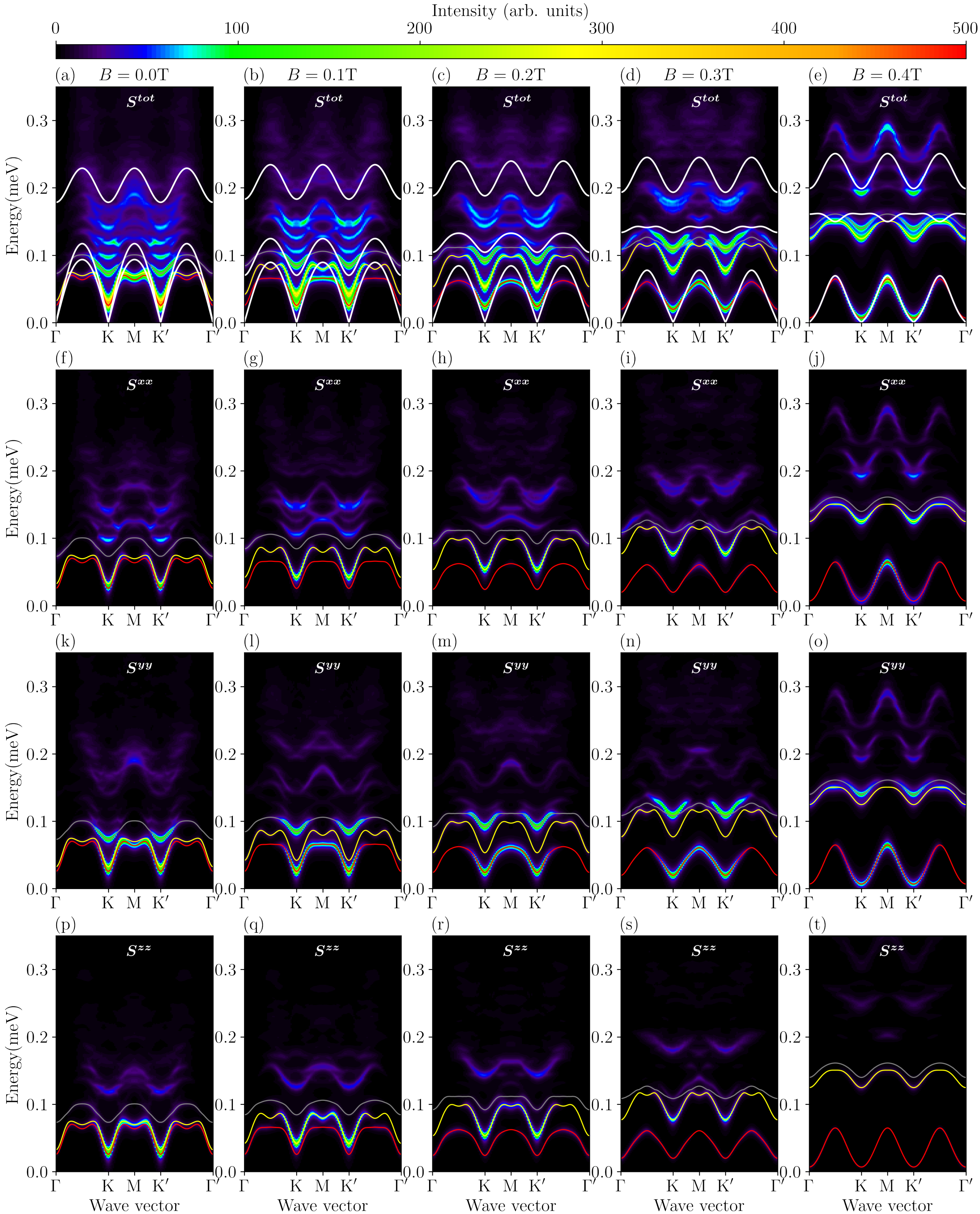

FIG. S4. The evolution of the dynamical spectral functions with magnetic field in the Y-shape phase. (a)-(e) The total spectral functions under magnetic fields of $B = 0.0, 0.1, 0.2, 0.3$ and 0.4 T, respectively. The white curves denote the LSWT results. (f)-(j) The spin x-component spectral function. (k)-(o) The spin y-component spectral function. (p)-(t) The spin z-component spectral function.

[R1] R. Chi, Y. Liu, Y. Wan, H.-J. Liao, and T. Xiang, Phys. Rev. Lett. **129**, 227201 (2022).

[R2] H.-J. Liao, J.-G. Liu, L. Wang, and T. Xiang, Phys. Rev. X **9**, 031041 (2019).

[R3] L. Vanderstraeten, M. Mariën, F. Verstraete, and J. Haegeman, Phys. Rev. B **92**, 201111 (2015).

[R4] L. Vanderstraeten, J. Haegeman, and F. Verstraete, Phys. Rev. B **99**, 165121 (2019).

[R5] B. Ponsioen and P. Corboz, Phys. Rev. B **101**, 195109 (2020).

[R6] B. Ponsioen, F. F. Assaad, and P. Corboz, SciPost Phys. **12**, 006 (2022).

[R7] W.-L. Tu, L. Vanderstraeten, N. Schuch, H.-Y. Lee, N. Kawashima, and J.-Y. Chen, PRX Quantum **5**, 010335 (2024).

[R8] J. Sheng, L. Wang, W. Jiang, H. Ge, N. Zhao, T. Li, M. Kofu, D. Yu, W. Zhu, J.-W. Mei, Z. Wang, and L. Wu, (2024), arXiv:2402.07730 [cond-mat.str-el].